Auxiliary material for Paper 2010GL045462

Remotely triggered microearthquakes and tremor in Central California following the 2010 Mw 8.8 Chile Earthquake

Zhigang Peng1, David P. Hill2, David R. Shelly2 and Chastity Aiken1

1. School of Earth and Atmospheric Sciences, Georgia Institute of Technology, Atlanta, Georgia
2. United States Geological Survey, Menlo Park, California

Geophys. Res. Lett., 37, L24312, doi:10.1029/2010GL045462, 2010.

Introduction

This auxiliary material contains a section called Supplementary Text, eight Supplementary figures, and their figure captions.

Supplementary Text

1. Data

The seismic data used in this study come from the High Resolution Seismic Network (HRSN) operated by Berkeley Seismological Laboratory, University of California, Berkeley, the Northern California Seismic Network (NCSN) operated by the U.S. Geological Survey, Menlo Park, and the Southern California Seismic Network (SCSN) operated by Caltech, and are distributed by the Northern and Southern California Earthquake Data Centers.

For the study in Coso we first download the SCSN catalog around the 2010 Chile mainshock from the Southern California Earthquake Data Center (SCEDC) within a rectangular area (longitudes between -118.25^{o} and -117.5^{o}, and latitudes between 35.75^{o} and 36.25^{o}) that bounds our study region. We also employ seismograms of the Chile earthquake recorded at the broadband station JRC2 (sensor type CMG-3ESP with a natural period of 120 s). This station is a replacement of (and close to) the station JRC that was used in identifying triggered earthquakes following the 2002 M_w7.8 Denali Fault earthquake [*Prejean et al.*, 2004].

For the triggered tremor around the Parkfield-Cholame section of the San Andreas Fault (SAF), we examine continuous waveforms around the Chile mainshock recorded at nearby surface stations that belong to the NCSN and Berkeley Digital Seismic Network (BDSN), and the borehole stations that belong to the HRSN. The station PKD belonging to the BDSN is equipped with STS-2 broadband sensor with a natural period of 120 s.

2. Seismicity rate change at Coso

We test the hypothesis that these events are triggered by the Chile mainshock by the following two procedures. First, we compare the seismicity rate immediately before and after the *P* wave of the Chile mainshock and compute the β-statistic value [*Matthews and Reasenberg*, 1988; *Kilb et al.*, 2002], which is a measure of the difference between the observed number of events after the main shock and the expected number from the averaged rate before the main shock. We calculate the β-value based on 15 days of seismicity before and within 1 hour after the theoretical arrival time of the *P* wave of the Chile mainshock. The resulting β-value is 21.9 for events with magnitude larger than 0.9, the magnitude of completeness based on the 90% goodness-of-fit test [*Wiemer and Wyss*, 2000]. If we change the pre-mainshock time window to be 90, 60, 30, 5, 1, and 0.25 day

(6 hour) before the *P* waves, the corresponding β-value are 20.7, 15.6, 26.7, 22.0, 11.45, and 12.82 respectively. The variations in the β-values originate from the fluctuations in the background seismicity. The reduction of the β-value with short pre-mainshock time is likely because the triggered activity occurred during an extended period of swarm activity in the CGF immediately before the mainshock. Nevertheless, because all these values are clearly above 2, we suggest that the increase of seismic activity immediately after the teleseismic *P* wave of the Chile mainshock is statistically significant [*Matthews and Reasenberg*, 1988; *Hill and Prejean*, 2007].

As shown above and mentioned in *Hill and Prejean* [2007], the β-statistic relies largely on the choice of the time window and could vary due to fluctuations in background seismicity. As an alternative approach, we use earthquakes listed in the SCSN between 1997/01/01 (approximate beginning time of the broadband station JRC) and 2010/08/25, and determine the likelihood of an $M_l \geq 3.45$ event and 4 $M_l \geq 2$ events within 1 hr occurring by random chance around Coso. The total numbers are 86 and 507, respectively, which correspond to the odds of seeing them for a given hour to be 0.07% and 0.42%, respectively (Figure S1). These numbers are calculated based on the assumption of random occurrence. Instead, the seismicity around Coso shows clear clustering around 1998, 2000-2002, and 2010. In particular, the seismicity rate around Coso in early 2010 was high, with two swarm-like sequences occurred around 2010/01/15 and the Chile mainshock. If we fix the time window to be between 01/12/2010 and 03/12/2010 (the approximate start and end of the most recent swarm-like sequences), the total numbers for an $M_l \geq 3.45$ event and 4 $M_l \geq 2$ events within 1 hr are 9 and 14, respectively, which correspond to the probability of occurring in any given hour to be 0.64% and 0.99%, respectively. Based on this, we can reject the hypothesis that these events occur by random chance at the 99% confidence level.

3. Seismicity rate change at Parkfield

Similar to the study in Coso, we calculate the β-value based on the 15 days of the low-frequency earthquakes (LFEs) around Parkfield before and within 1 hour after the arrival time of the *P* wave of the Chile mainshock. The resulting β-value is 18.3. If we change the pre-mainshock time window to be 90, 60, 30, 5, 1, and 0.25 day (6 hour) before the *P* waves, the corresponding β-value are 8.9, 8.6, 18.2, 26.1, 43.4, and 101.0, respectively. Again, the variations in the β-values originate from the fluctuations in the background LFEs. The increase of the β-value with short pre-mainshock time is likely because the rate of LFEs around Parkfield immediately before the Chile mainshock is relatively small. Nevertheless, because all these values are clearly above 2, we suggest that the increase of LFE activity immediately after the teleseismic *P* wave of the Chile mainshock is statistically significant [*Matthews and Reasenberg*, 1988; *Hill and Prejean*, 2007]. If we keep the pre-mainshock time window as 15 day and increase the post-mainshock time window to 15 day, the β-value decreases to -0.48, again suggesting that the seismicity increase following the Chile mainshock is statistically significant only within a short time window.

4. Correlations between the surface waves and triggered activity

We shift both the surface waves and the locally triggered signals back to the source region to evaluate their correlations. For the Coso case, the distance between the M_l 3.5

event and the station JRC2 is 11.3 km. Assuming the Love wave velocity of 4.3 km/s, we shift the transverse component seismogram forward by ~2.6 s to reflect the timing at the epicenter of the M_l 3.5 event. The time difference between the peak of the Love wave (open circle) and the origin time of the M_l 3.5 event is 15.7 s (Figure 3b). Figure S7 shows that the first two earthquakes with M_l = 2.9 and 2.1 occurred ~51 s before and ~249 s after the *S* arrival predicted from the iasp91 global velocity model [*Kennett and Engdahl*, 1991], respectively. The last M_l = 2.3 event occurred ~436 s after the long-period Rayleigh waves with the velocity of 3.8 km/s. We did not apply any time shifts in calculating these time differences.

For the SAF case, we first compute the average location of 33 low-frequency earthquakes (LFEs) occurred between 2200 and 3000 s: ($-120.2489^o \pm 0.04^o$, $35.6830^o \pm 0.04^o$, and depth 23.6 ± 1.5 km). Next, we compute the *S*-wave travel time based on the 1D velocity in this region [*Peng et al.*, 2009], and shift the 15-30 Hz band-pass-filtered seismogram at station GHIB backward by 9.25 s to the tremor source region. The transverse component seismogram has been time shifted backward by 9.15 s with the Love wave velocity of 4.3 km/s, and the radial and vertical component seismograms are time shifted backward by 10.3 s with the Rayleigh wave velocity of 3.8 km/s.

5. Theoretical assessment of the triggering potential

We model the triggering potential of the Rayleigh and Loves following the procedure of *Hill* [2008, 2010]. For the Coso case, we choose the focal depth to be $z \sim 2.0$ km, close to the focal depth of the 4 triggered microearthquakes as listed in the SCSN catalog. We assume an intermediate value of coefficient of friction $\mu^* = 0.4$, although the actual value could be lower due to the existence of elevated fluid pressure at shallow depth [*Bhattacharyya and Lees*, 2002].

The focal mechanism for the M_l = 3.5 Coso earthquake triggered by surface waves from the Chile earthquake is not well constrained. In the main text we calculated the potential for Love and Rayleigh wave triggering dextral slip on a north-striking vertical fault consistent with the mapped faults and seismicity patterns in the vicinity of the epicenter [*Roquemore*, 1982; *Feng and Lees*, 1998]. In Figure S5 we compute the triggering potential for fault orientations based on three focal mechanisms: one from the Southern California Seismic Network (W. Yang, personal communication, 2010) and two from the local Coso seismic network operated by the Naval Weapons Center (W.-C. Huang, personal communication, 2010). The Love wave triggering potential is four times the Rayleigh wave potential for the SCSN solution (Figure S5a), and comparable to that for Rayleigh wave for the mechanism from the Naval Weapons Center network (Figure S5b,c). In all three cases, however, the δCF stresses corresponding to wave incidence from Chile are less than half those for the vertical fault in Figure 4a. We do not use these mechanisms in the main text because of the large uncertainties in the solutions (W. Yang and W.-C. Huang, personal communication, 2010).

For the SAF case, we calculate the triggering potential on a vertical strike-slip fault (with strike direction of 140^o clockwise from north) at the depth of $z \sim 25$ km with a low apparent coefficient of friction $\mu^* = 0.2$, which is likely reasonable for the source region where tremor and LFEs occur [*Peng et al.*, 2009; *Thomas et al.*, 2009]. We have also tested other μ^* values and found that as the friction coefficient decreases, the triggering potential curves for both the Love and Rayleigh waves become more symmetric about the

0-degree incident angle (Figure S6). In all the cases, however, the Love wave has larger triggering potential than the Rayleigh wave for incidence on the SAF at depths of ~25 km assuming equal Love- and Rayleigh-wave displacement amplitudes as the surface (z = 0 km).

6. References that are cited here but not in the main text:

Kennett, B. L. N., E. R. Engdahl (1991), Traveltimes for global earthquake location and phase identification, *Geophys. J. Intl.*, 105, 429-465.

Matthews, M. V., and P. A. Reasenberg (1988), Statistical methods for investigating quiescence and other temporal seismicity patterns, *Pure Appl. Geophys.*, 126, 357-372.

Prejean, S. G., D. P. Hill, E. E. Brodsky, S. E. Hough, M. J. S. Johnston, S. D. Malone, D. H. Oppenheimer, A. M. Pitt, and K. B. Richards-Dinger (2004), Remotely triggered seismicity on the United States west coast following the Mw 7.9 Denali fault earthquake, Bull. Seismol. Soc. Am., 94, S348 – S359, doi:10.1785/0120040610.

Roquemore, G. R. (1982), Reconnaissance geology and structure of the Coso Range, California; Naval Weapons Center Tech. Pub. 6036, 26 p., 2 plates.

Thomas, A. M., R. M. Nadeau and R. Bürgmann (2009), Tremor-tide correlations and near-lithostatic pore pressure on the deep San Andreas fault, *Nature*, 462, 1048-1051.

Wiemer, S. and M. Wyss (2000), Minimum magnitude of completeness in earthquake catalogues: examples from Alaska, the western United States, and Japan, *Bull. Seismol. Soc. Am.*, 90, 859–869.

Supplementary Figures

Figure S1. (a) Magnitudes versus occurrence times for all earthquakes occurred around the Coso region since 1997. The red circles mark the events with $M_l \geq 3.45$ event, and the green dashed lines mark the time when at least 4 $M_l \geq 2$ events occurred within 1 hr. The green circle marks the M_l = 3.5 event occurred during the Love wave of the Chile mainshock. (b) A zoom-in plot of (a) around 2009-2010. The two gray dashed lines mark the approximate start (01/12/2010) and end (03/12/2010) of the most recent swarm sequences. (c) Magnitudes versus the time relative to the origin time of the Chile mainshock (solid vertical line) for all earthquakes.

Figure S2. A record section of the 2-8 Hz band-pass-filtered vertical seismograms showing regionally triggered earthquakes and locally triggered tremor by the 2010 M_w8.8 Chile earthquake in the Parkfield region, and the broadband three-component velocity seismograms recorded at station PKD. The seismograms are plotted according to the along-strike distances on the SAF, which are marked on the left hand side together with the station and channel names. The vertical dashed lines mark the original times of the four microearthquakes occurred near Coso. The gray and open vertical arrows mark the predicted arrivals of the Love (with the phase velocity of 4.3 km/s) and Rayleigh waves (with the phase velocity of 3.8 km/s) at station PKD.

Figure S3. A record section of 2-16 Hz band-pass-filtered vertical seismograms showing the moveout of the M_l 3.5 earthquake near Coso. The blue and red lines correspond to the seismic recordings at stations JRC2 and PKD, respectively. The green lines correspond to

the seismic recordings at stations around the Parkfield-Cholame section of the San Andreas Fault other than the PKD station.

Figure S4. A zoom-in plot of Figure S1 showing locally triggered tremor modulated with the Rayleigh waves of the 2010 M_w8.8 Chile earthquake.

Figure S5. Triggering potential for 200-second Love and Rayleigh waves in terms of the dynamic Coulomb-failure stress, δCF(γ) for Love (LW, solid line) and Rayleigh (RW, dashed line) waves as a function of incidence angle with respect to fault strike from the Mw 8.8 Chile earthquake for incidence on three first-motion fault-plane (FP) solutions for the M 3.4 earthquake at at a depth of ~ 2 km beneath Coso. (a) FP solution from the Southern California Seismic Network, (*Wenzheng Yang*, personal communication, 2010). (b) and (c) alternative FP solutions from the Coso GPO network (*Wei-Chuang Huang*, personal communication 2010). The peak dynamic stresses at 2 km are based on observed transverse and vertical displacement amplitudes for 200-s surface waves of 3.7 and 1.3 cm on station JRC2. The vertical line indicates the incidence angel of waves from the Chile earthquake with respect to the respective fault strikes. Rake is assumed to be parallel with the maximum resolved shear stress component of the regional stress field on the respective fault planes.

Figure S6. Influence of variations in the coefficient of friction on the Love (solid line) and Rayleigh wave (dashed line) triggering potentials, P(γ), as a function of incidence angle on the San Andreas Fault (SAF) computed for a depth of 25 km as in Figure 4. Here, the dimensionless potential P(γ) is normalized by the peak Love wave dynamic stress δCF(γ) = 3.3 kPa. Note that the peaks and nulls in the Love wave potential are shifted to the right (increasing incidence angles) with increasing friction and Rayleigh wave potential becomes progressively more asymmetric about zero (strike-parallel) incidence with increasing friction. The vertical line marks the incidence angle for waves from the Chile earthquake.

Figure S7. (a) A zoom-in plot of Figure 3a showing the relationship between the teleseismic body waves of the Chile mainshock and the local earthquakes near Coso. The origin times of these two local events are marked by the gray lines. The vertical dashed line mark the predicted S arrival of the Chile earthquake. (b) A zoom-in plot of Figure 3a showing the relationship between the surface waves of the Chile mainshock and the local earthquakes near Coso.

Figure S8. A zoom-in plot showing the relationships among the Love waves of the Chile mainshock, the regional seismic signals from the M_l 3.5 earthquake near Coso, and high-frequency local tremor signals. All the traces have been time shifted to reflect their relationship at the tremor source region.

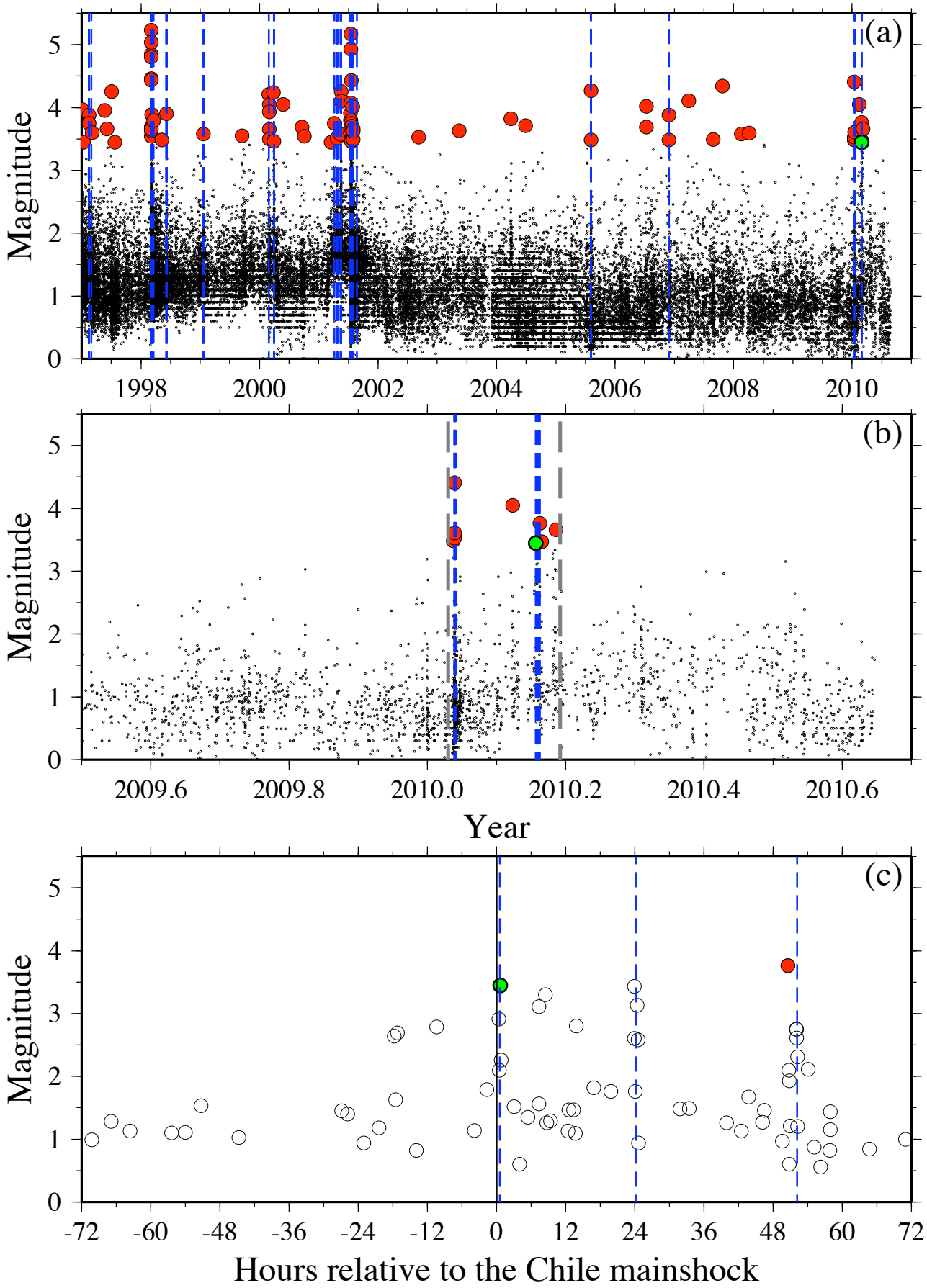
(a)
Magnitude
0
1
2
3
4
5
1998
2000
2002
2004
2006
2008
2010
(b)
Magnitude
2009.6
2009.8
2010.0
2010.2
2010.4
2010.6
Year
(c)
Magnitude
-72
-60
-48
-36
-24
-12
0
12
24
36
48
60
72
Hours relative to the Chile mainshock

Figure S1

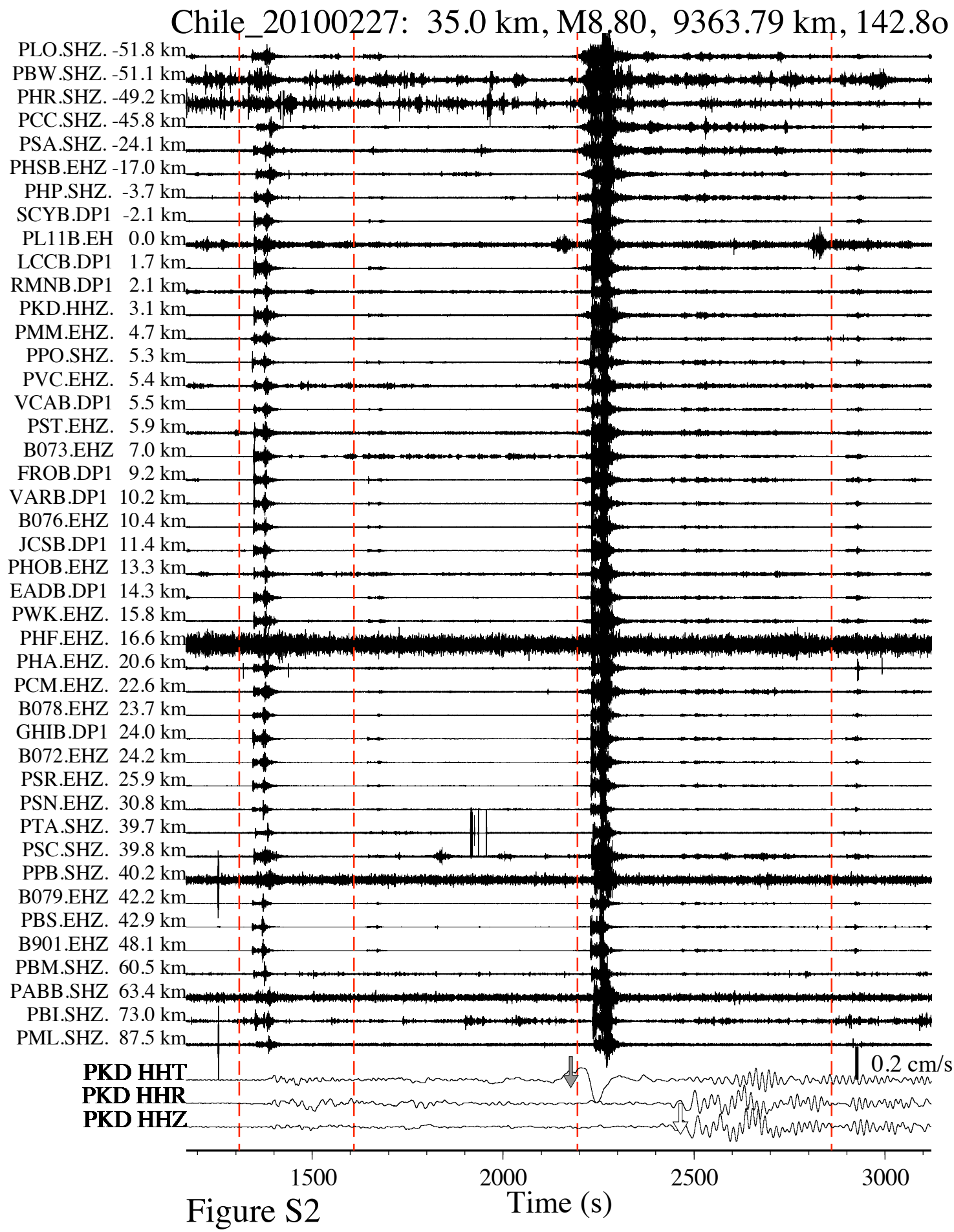
Chile_20100227: 35.0 km, M8.80, 9363.79 km, 142.8o
PLO.SHZ. -51.8 km
PBW.SHZ. -51.1 km
PHR.SHZ. -49.2 km
PCC.SHZ. -45.8 km
PSA.SHZ. -24.1 km
PHSB.EHZ -17.0 km
PHP.SHZ. -3.7 km
SCYB.DP1 -2.1 km
PL11B.EH 0.0 km
LCCB.DP1 1.7 km
RMNB.DP1 2.1 km
PKD.HHZ. 3.1 km
PMM.EHZ. 4.7 km
PPO.SHZ. 5.3 km
PVC.EHZ. 5.4 km
VCAB.DP1 5.5 km
PST.EHZ. 5.9 km
B073.EHZ 7.0 km
FROB.DP1 9.2 km
VARB.DP1 10.2 km
B076.EHZ 10.4 km
JCSB.DP1 11.4 km
PHOB.EHZ 13.3 km
EADB.DP1 14.3 km
PWK.EHZ. 15.8 km
PHF.EHZ. 16.6 km
PHA.EHZ. 20.6 km
PCM.EHZ. 22.6 km
B078.EHZ 23.7 km
GHIB.DP1 24.0 km
B072.EHZ 24.2 km
PSR.EHZ. 25.9 km
PSN.EHZ. 30.8 km
PTA.SHZ. 39.7 km
PSC.SHZ. 39.8 km
PPB.SHZ. 40.2 km
B079.EHZ 42.2 km
PBS.EHZ. 42.9 km
B901.EHZ 48.1 km
PBM.SHZ. 60.5 km
PABB.SHZ 63.4 km
PBI.SHZ. 73.0 km
PML.SHZ. 87.5 km
PKD HHT
PKD HHR
PKD HHZ
0.2 cm/s
1500
2000
2500
3000
Time (s)

Figure S2

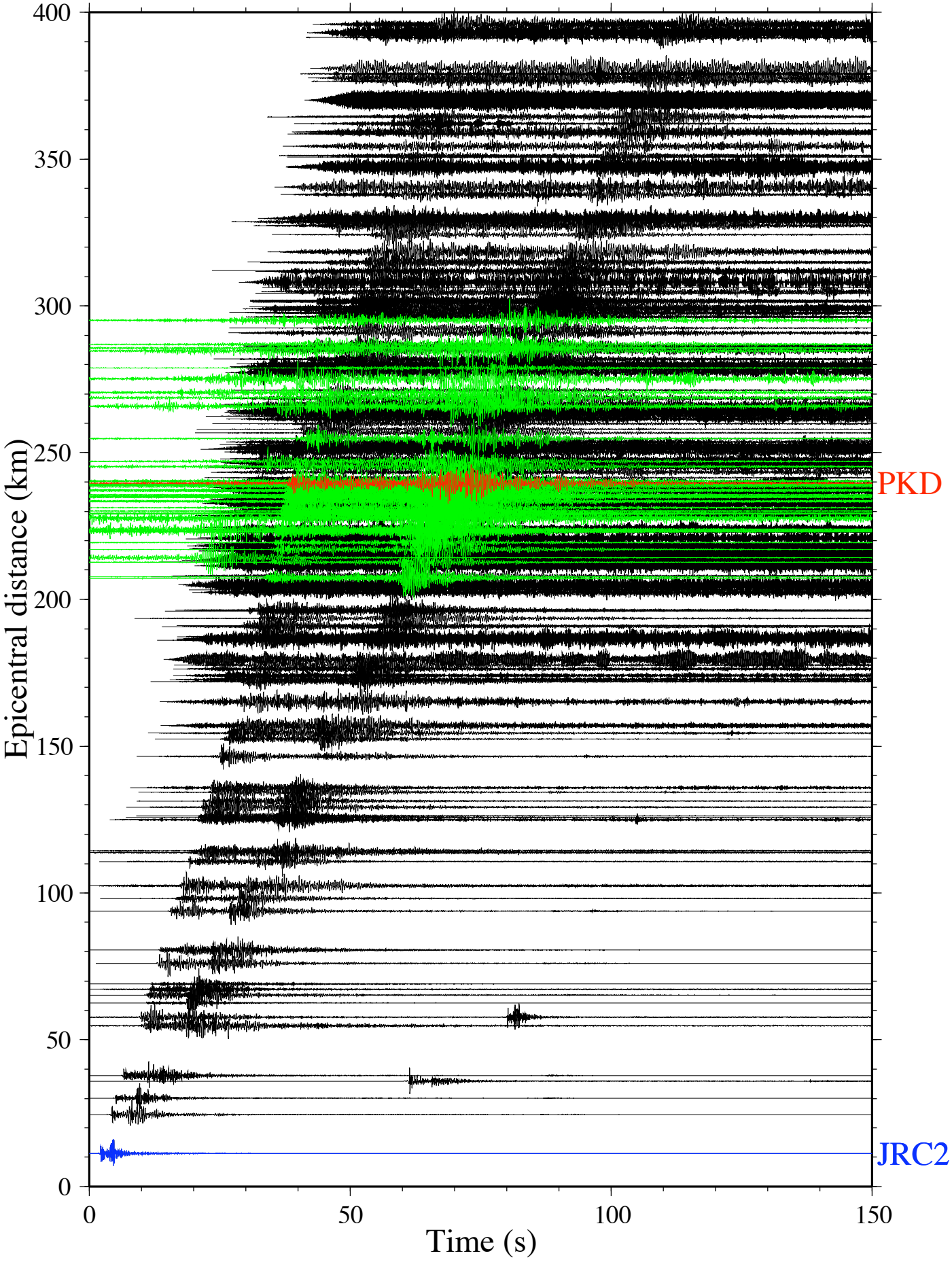
400
350
300
250
200
150
100
50
0
Epicentral distance (km)
PKD
JRC2
0
50
100
150
Time (s)

Figure S3

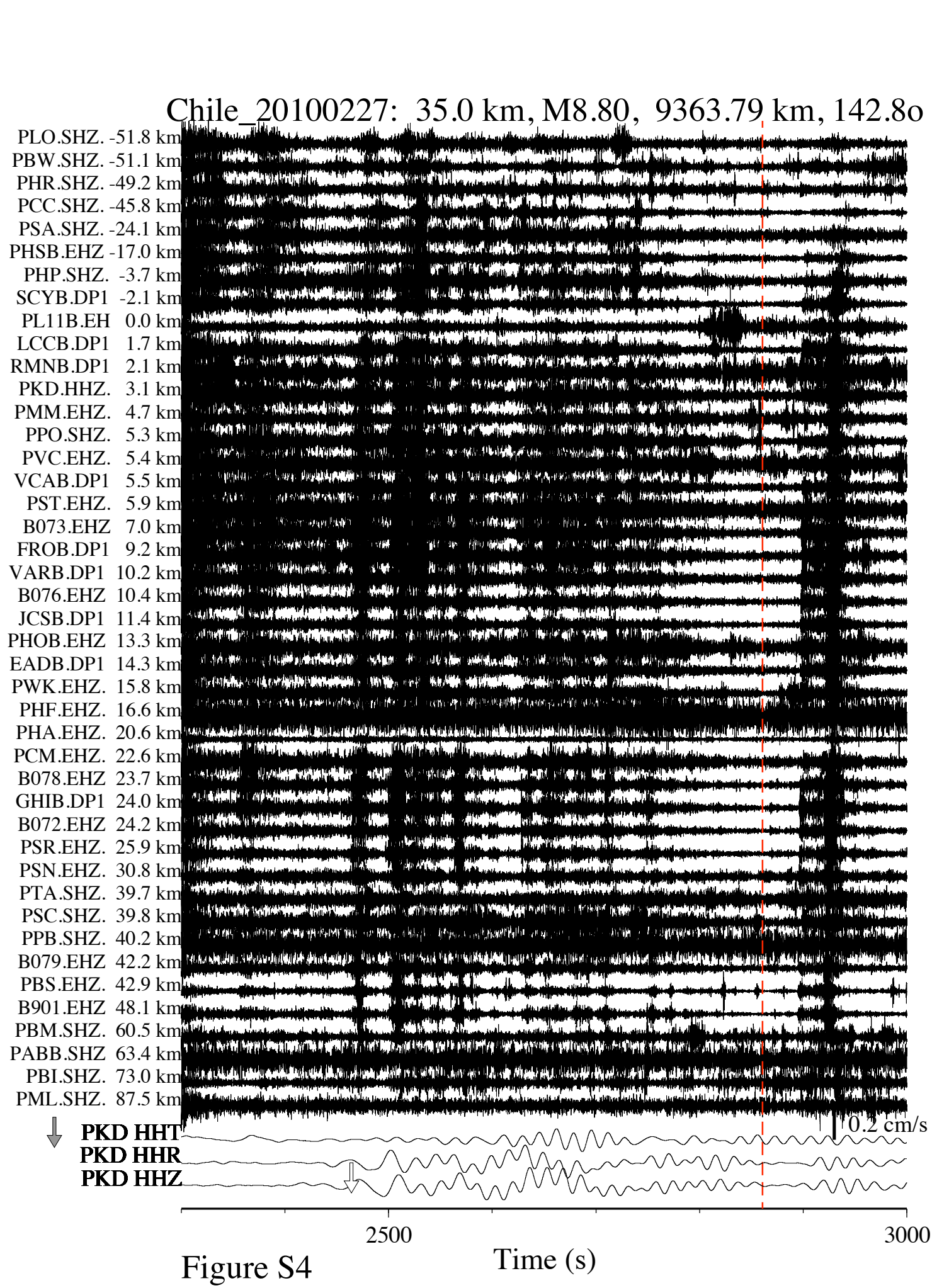
Chile_20100227: 35.0 km, M8.80, 9363.79 km, 142.8o
PLO.SHZ. -51.8 km
PBW.SHZ. -51.1 km
PHR.SHZ. -49.2 km
PCC.SHZ. -45.8 km
PSA.SHZ. -24.1 km
PHSB.EHZ -17.0 km
PHP.SHZ. -3.7 km
SCYB.DP1 -2.1 km
PL11B.EH 0.0 km
LCCB.DP1 1.7 km
RMNB.DP1 2.1 km
PKD.HHZ. 3.1 km
PMM.EHZ. 4.7 km
PPO.SHZ. 5.3 km
PVC.EHZ. 5.4 km
VCAB.DP1 5.5 km
PST.EHZ. 5.9 km
B073.EHZ 7.0 km
FROB.DP1 9.2 km
VARB.DP1 10.2 km
B076.EHZ 10.4 km
JCSB.DP1 11.4 km
PHOB.EHZ 13.3 km
EADB.DP1 14.3 km
PWK.EHZ. 15.8 km
PHF.EHZ. 16.6 km
PHA.EHZ. 20.6 km
PCM.EHZ. 22.6 km
B078.EHZ 23.7 km
GHIB.DP1 24.0 km
B072.EHZ 24.2 km
PSR.EHZ. 25.9 km
PSN.EHZ. 30.8 km
PTA.SHZ. 39.7 km
PSC.SHZ. 39.8 km
PPB.SHZ. 40.2 km
B079.EHZ 42.2 km
PBS.EHZ. 42.9 km
B901.EHZ 48.1 km
PBM.SHZ. 60.5 km
PABB.SHZ 63.4 km
PBI.SHZ. 73.0 km
PML.SHZ. 87.5 km
PKD HHT
PKD HHR
PKD HHZ
0.2 cm/s
2500
3000
Time (s)

Figure S4

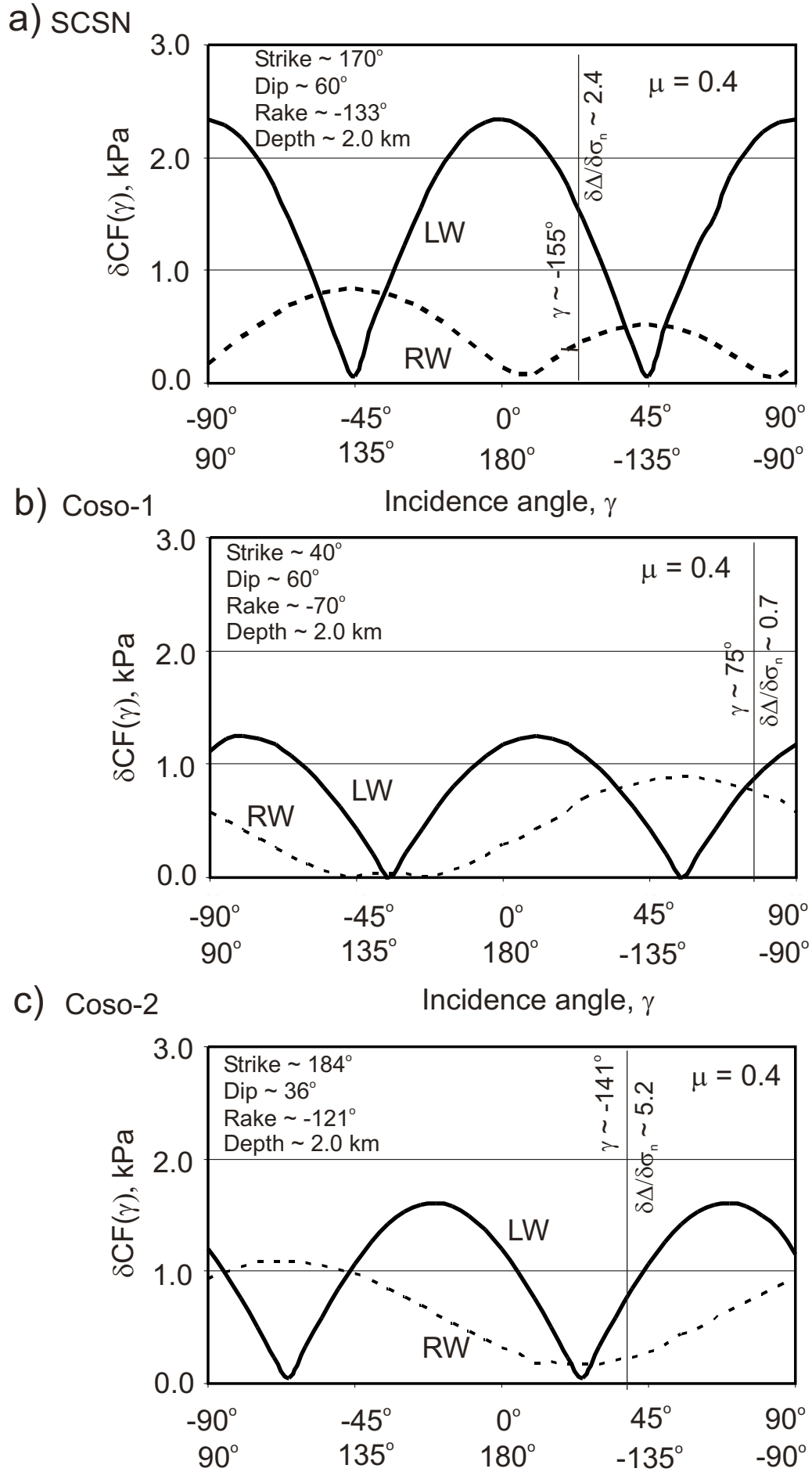
a) SCSN
Strike ~ 170°
Dip ~ 60°
Rake ~ -133°
Depth ~ 2.0 km
μ = 0.4
δΔ/δσn ~ 2.4
γ ~ -155°
LW
RW
δCF(γ), kPa
3.0
2.0
1.0
0.0
-90° 90°
-45° 135°
0° 180°
45° -135°
90° -90°
Incidence angle, γ
b) Coso-1
Strike ~ 40°
Dip ~ 60°
Rake ~ -70°
Depth ~ 2.0 km
μ = 0.4
γ ~ 75°
δΔ/δσn ~ 0.7
LW
RW
δCF(γ), kPa
3.0
2.0
1.0
0.0
-90° 90°
-45° 135°
0° 180°
45° -135°
90° -90°
Incidence angle, γ
c) Coso-2
Strike ~ 184°
Dip ~ 36°
Rake ~ -121°
Depth ~ 2.0 km
μ = 0.4
γ ~ -141°
δΔ/δσn ~ 5.2
LW
RW
δCF(γ), kPa
3.0
2.0
1.0
0.0
-90° 90°
-45° 135°
0° 180°
45° -135°
90° -90°

Figure S5

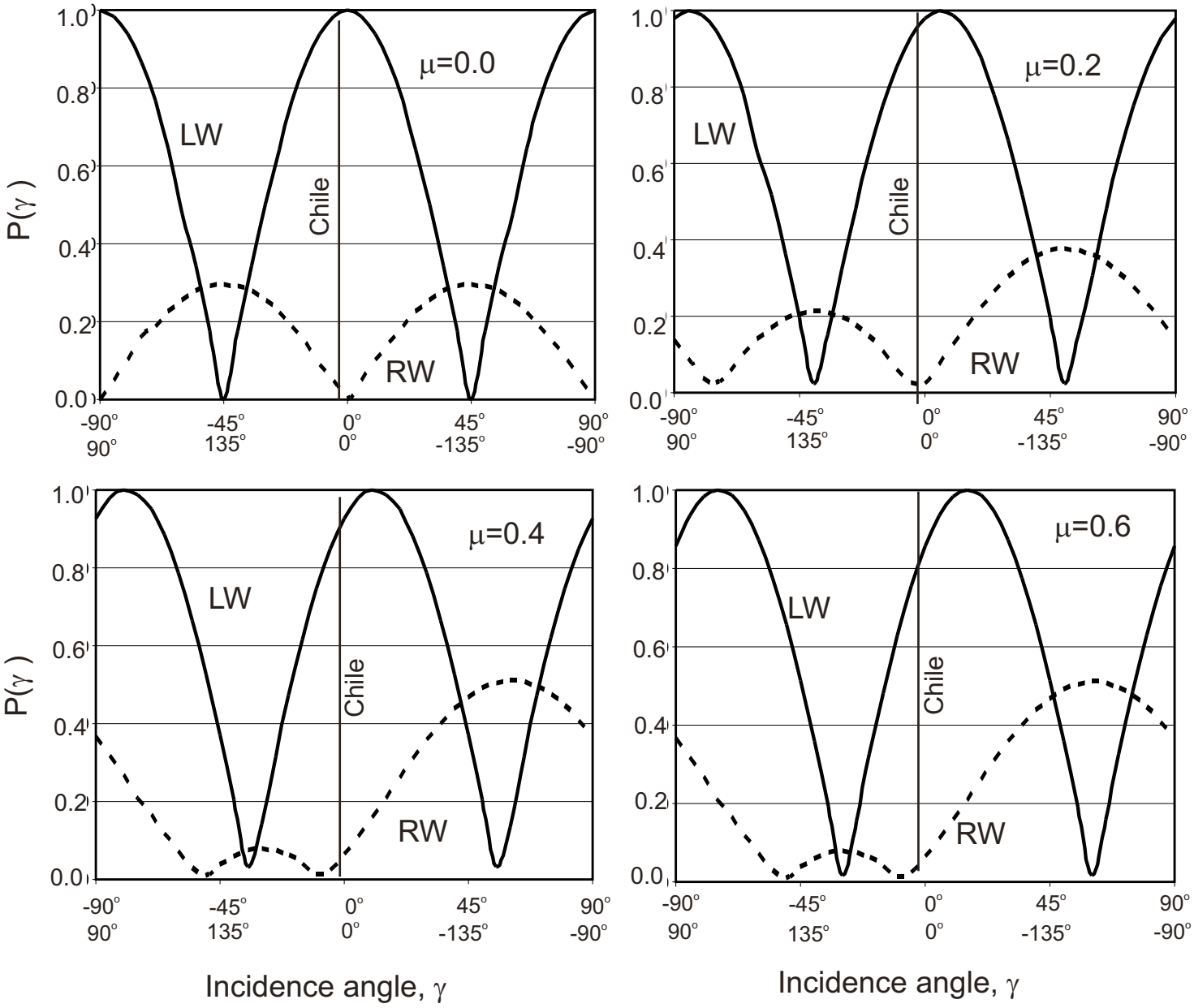
μ=0.0
μ=0.2
μ=0.4
μ=0.6
LW
RW
Chile
P(γ)
1.0
0.8
0.6
0.4
0.2
0.0
-90°
90°
-45°
135°
0°
0°
45°
-135°
90°
-90°
Incidence angle, γ

Figure S6

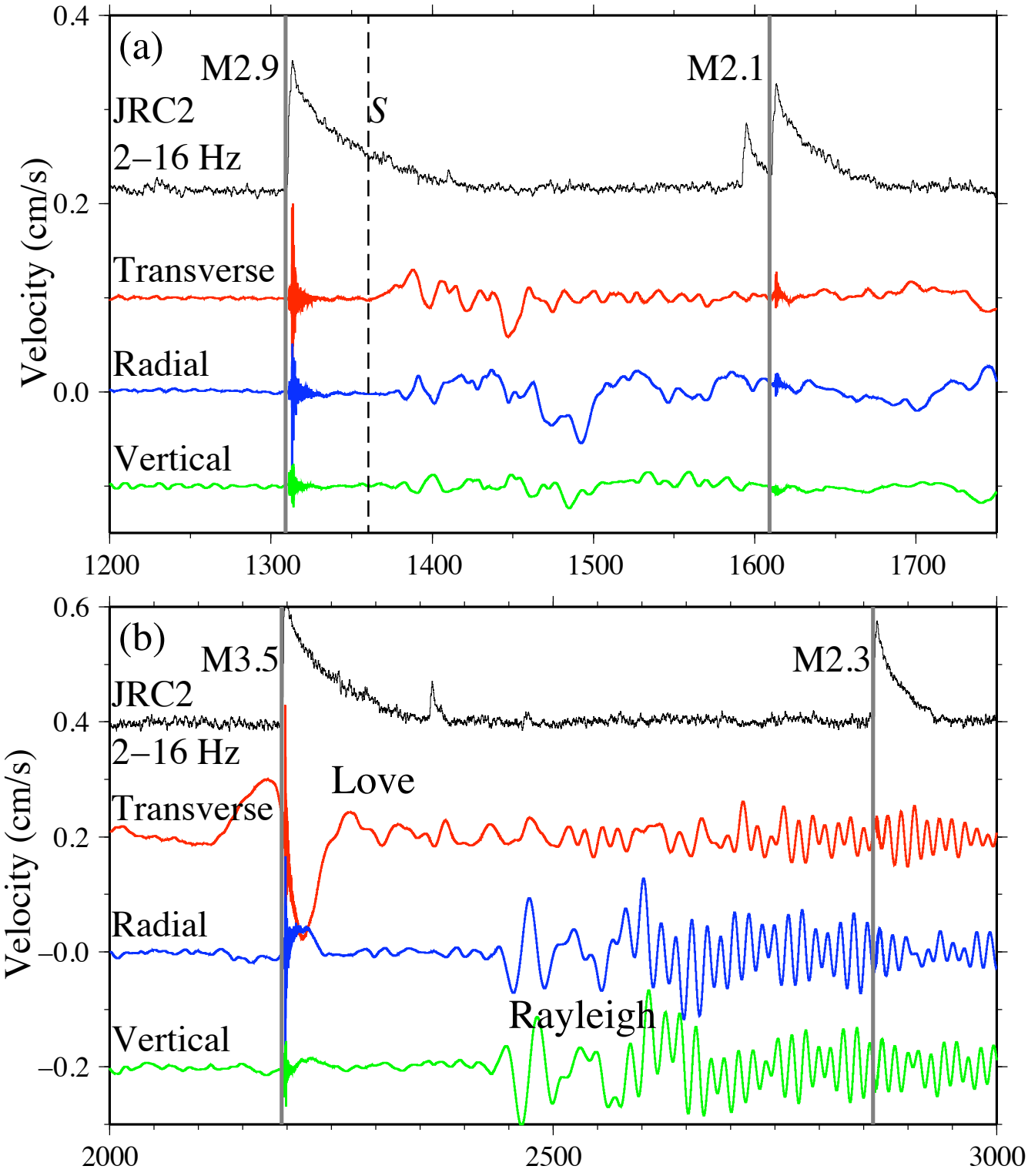
(a)
M2.9
M2.1
S
JRC2
2–16 Hz
Transverse
Radial
Vertical
Velocity (cm/s)
0.4
0.2
0.0
1200
1300
1400
1500
1600
1700
(b)
M3.5
M2.3
JRC2
2–16 Hz
Transverse
Love
Radial
Rayleigh
Vertical
Velocity (cm/s)
0.6
0.4
0.2
–0.0
–0.2
2000
2500
3000

Figure S7

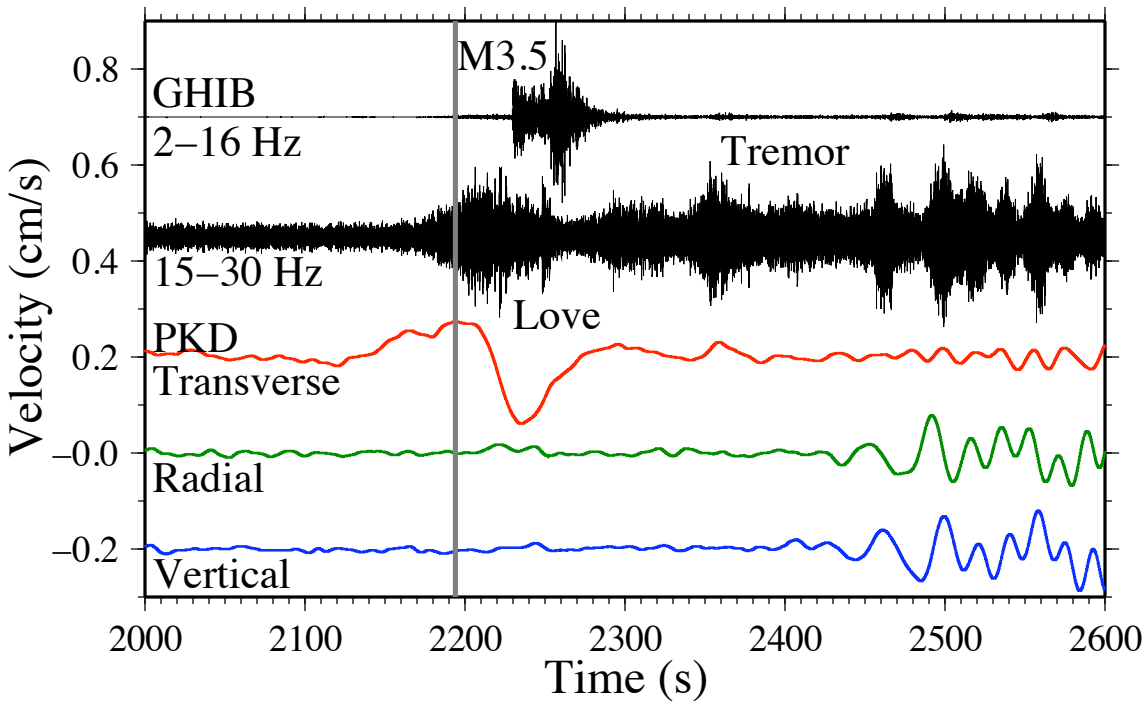
M3.5
GHIB
2–16 Hz
Tremor
15–30 Hz
Love
PKD
Transverse
Radial
Vertical
0.8
0.6
0.4
0.2
–0.0
–0.2
Velocity (cm/s)
2000
2100
2200
2300
2400
2500
2600
Time (s)

Figure S8